

On the nature of the triplet electronic states of naphthalene dimers.

Supporting Information

1. Experimental methods

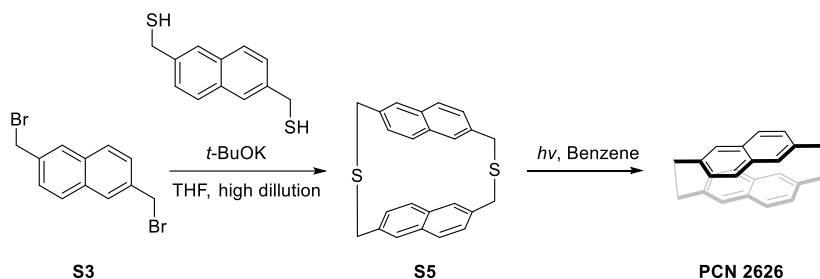
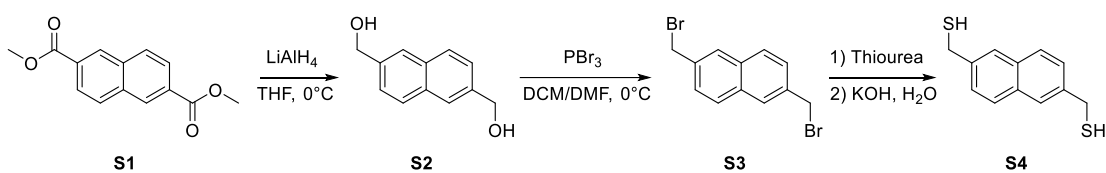
1.1. Synthesis

All reagents were commercially available and used as supplied without further purification, compounds **S1** – **S11**, **PCN 2626**, **PCN 1526**, **PCN 1515 cross** and **PCN 1515** were prepared according to the published method.¹

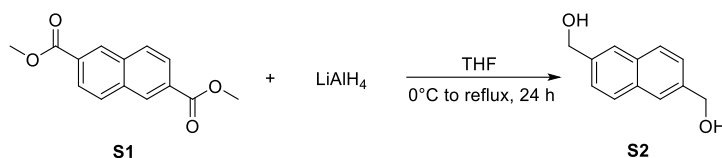
² In brief, bis(bromomethyl)naphthalene **S3** was derived from the continuous functional group transformation of commercial reagent **S1**. Bis(bromomethyl)naphthalene **S8** was obtained from the bromination reaction of commercial reagent **S7**. Bis(mercaptomethyl)naphthalenes were obtained from the continuous functional group transformation from the bis(bromomethyl)naphthalenes, respectively. Thioethers as a precursor of naphthalene dimers were synthesized by cyclization reaction between bis(bromomethyl)naphthalene and bis(mercaptomethyl)naphthalene, respectively. In order to reduce the polymer in the cyclization reaction, the reaction was carried out under high dilution conditions. Benzene was used as solvent and triethyl phosphite as additive in the photolysis desulfurization reaction. All naphthalene dimers have been identified for their precise structure through X-ray single crystal diffraction. Deuterated solvents were purchased from Cambridge Isotope Laboratory (Andover, MA).

All solvents were dried according to standard procedures and all of them were degassed under N₂ for 30 minutes before use. All air-sensitive reactions were carried out under inert N₂ atmosphere. ¹H NMR and ¹³C NMR spectra were recorded on Bruker 400 MHz Spectrometer (¹H: 400 MHz; ¹³C: 100 MHz). The ¹H and ¹³C NMR chemical shifts are reported relative to residual solvent signals. The high-resolution electron spray ionization mass spectra (HR ESI-MS) were performed on an Agilent (Santa Clara, CA, USA) ESI-TOF mass spectrometer (6224) and micrOTOF mass spectrometer. Separation of isomers for **PCN 1515 cross** and **PCN 1515** was performed using a Shimadzu HPLC System (LC-20AR) equipped with a CHIRALPAK IF[®] column (250 mm L × 10 mm I. D. for separation and 250 mm L × 4.6 mm I. D. for analysis) and eluting at flow rates of 3.0 mL/min for separation and 1.0 mL/min for analysis.

1.1.1. Synthesis and characterization of PCN 2626.

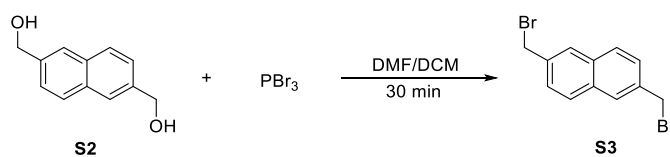


1.1.1.1. Synthesis of S2:



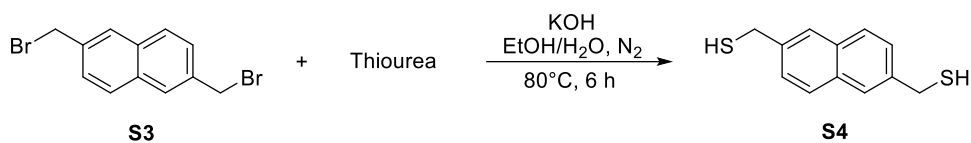
In the ice water bath, LiAlH₄ (0.76 g, 0.02 mol) suspended in 30 mL of THF was transferred slowly to a solution of **S1** (2.44 g, 0.01 mol) in 50 mL of THF. The mixture was stirred for 30 min at 0 °C and then at room temperature for another 30 min. The reaction was refluxed at 70 °C for 24 h. The mixture was cooled to room temperature and the excess LiAlH₄ was quenched by methanol. After removal of the solvents under reduced pressure, dilute hydrochloric acid (1 M, 30 mL) and ethyl acetate were added to extract the product. The organic layer was separated. Evaporation of the solvent gave **S2** as a white solid. Yield: 1.88 g (85%).

1.1.1.2. Synthesis of S3:



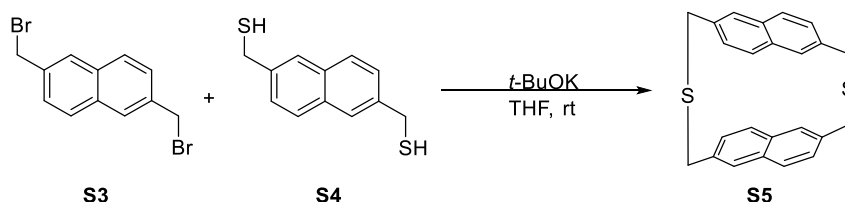
In ice water bath, PBr₃ (1.35 g, 5 mmol) was transferred dropwise to a solution of **S2** (0.94 g, 5 mmol) in 20 mL CH₂Cl₂ mixed with DMF (v: v = 3:1). After 30 min stirring, water of 20 mL was added. The aqueous layer was extracted with CH₂Cl₂. The organic layer was evaporated by rotavapor, producing a light-yellow solid. This crude product was washed with diethyl ether and collected by filtration. The product was dried under vacuum. Yield: 80%, 1.25 g.

1.1.1.3. Synthesis of **S4**:



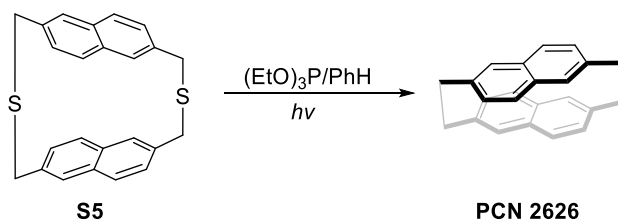
S3 (6.87 g, 13.7 mmol) was refluxed with thiourea (2.6 g, 33 mmol) in 100 ml of ethanol. The resulting solid was collected by filtration and potassium hydroxide (9 g, 0.16 mol) in 200 ml of water for 6 h under N₂. After the insoluble material was removed by filtration, the filtrate was acidified with 50% sulfuric acid on ice-cooling. The resulting solid was collected by filtration and recrystallized from chloroform to give **S4** white scales, 2.64 g, yield 62%.

1.1.1.4. Synthesis of **S5**:



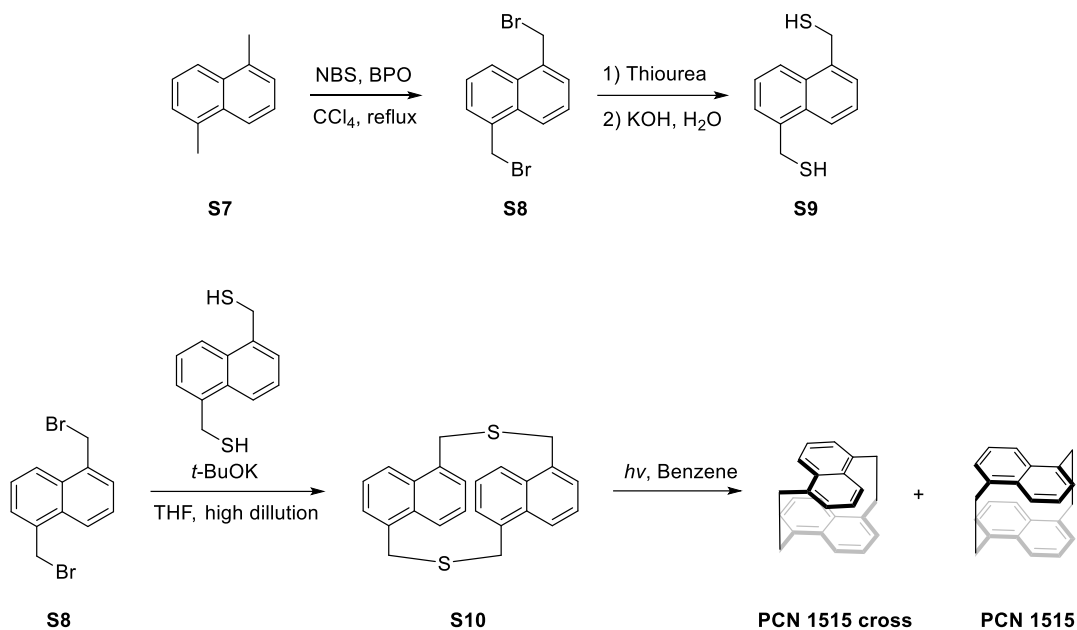
A solution of **S3** 156 mg (0.50 mmol) and **S4** 110 mg (0.50 mmol) in 40 ml dry THF was slowly added into a solution of THF (80 ml) containing *t*-BuOK in a nitrogen atmosphere under room temperature. The addition took 15 h. The solution was concentrated in vacuo, and the residue was chromatographed on silica gel with dichloromethane to give the desired product **S5** in the first eluate, 82 mg, yield: 44%, white solid.

1.1.1.5. Synthesis of **PCN 2626**:

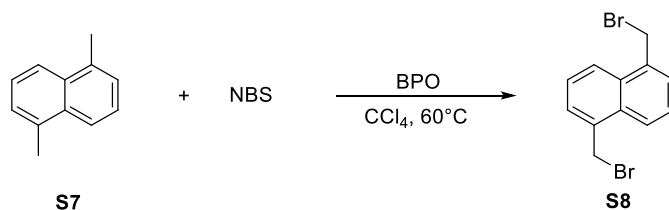


S5 93 mg, triethyl phosphite 10 ml, and benzene 15 ml were placed in a quartz tube. The suspension was irradiated with a 6W UV lamp for 12 h in a nitrogen atmosphere. It was evaporated, and the residue was purified and column chromatography on silica gel with chloroform to give the desired product **PCN 2626**, 25 mg (33%), white solid.

1.1.2. Synthesis and characterization of PCN 1515 and PCN 1515 cross.

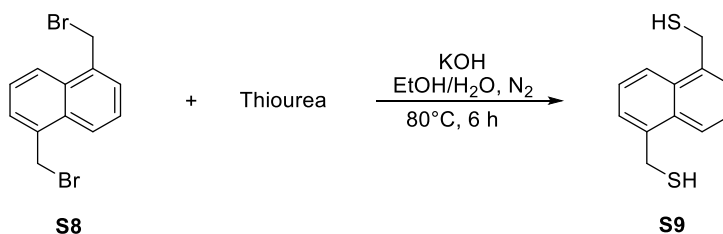


1.1.2.1. Synthesis of S8:



S7 780 mg (5 mmol) was refluxed with *N*-bromosuccinimide 1.78 g (10 mmol) and a catalytic amount of benzoyl peroxide in 20 ml of carbon tetrachloride for 12 h. After the reaction finish completely, the solution was concentrated in vacuo and the residue was washed with hot water. The resulting solid was recrystallized from methanol to give **S8** 1.2 g white powder in 67% yield.

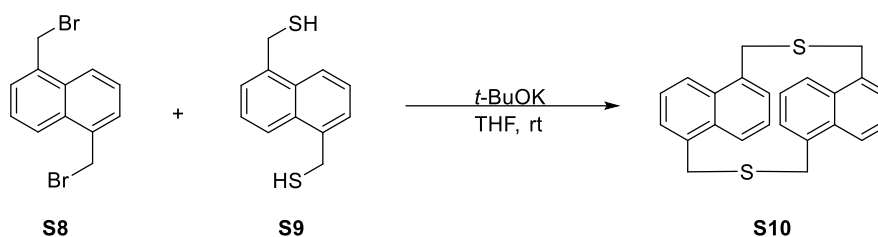
1.1.2.2. Synthesis of S9:



S8 (1.5 g, 5 mmol) was refluxed with thiourea (9.5 g, 12.5) in 80 ml of ethanol. The resulting solid was collected by filtration and potassium hydroxide (4.5 g, 80 mmol) in 160 ml of water for 3 h under N_2 . After the insoluble material was removed by filtration, the filtrate was acidified with 50% sulfuric acid on ice-cooling.

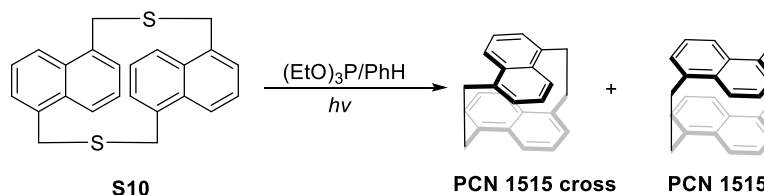
The resulting solid was collected by filtration and recrystallized from chloroform to give **S9** white scales, 0.88 g, yield 80%.

1.1.2.3. Synthesis of **S10**:

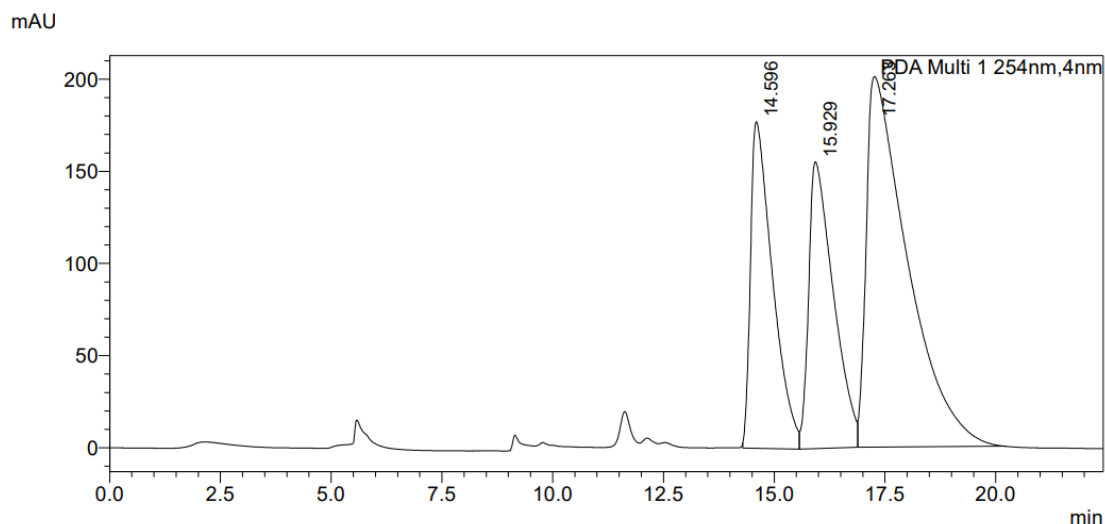


A solution of **S8** 156 mg (0.50 mmol) and **S9** 110 mg (0.50 mmol) in 40 ml dry THF was slowly added into a solution of THF (80 ml) containing *t*-BuOK in a nitrogen atmosphere under room temperature. The addition took 15 h. The solution was concentrated in vacuo, and the residue was chromatographed on silica gel with dichloromethane to give the desired product **S10** in the first eluate, 78 mg, yield: 43%, white solid.

1.1.3. Synthesis of PCN 1515 and PCN 1515 cross:



S10 90 mg (0.24 mmol), triethyl phosphite 10 ml, and benzene 15 ml were placed in a quartz tube. The suspension was irradiated with a 6W UV lamp for 12 h in a nitrogen atmosphere. It was evaporated, and the residue was purified by high performance liquid chromatography to give the desired product **PCN 1515 cross** and **PCN 1515**, 8 mg (11%) and 12 mg (15%) respectively, white solid.



<Peak Table>

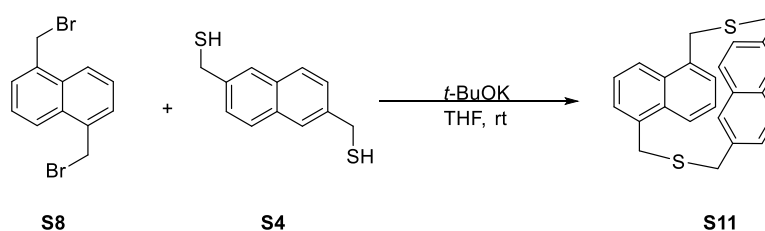
PDA Ch1 254nm

Peak#	Ret. Time	Area	Height	Conc.	Unit	Mark	Name
1	14.596	6129514	177271	0.000		M	
2	15.929	6051381	155642	0.000		M	
3	17.263	13010767	200985	0.000		M	
Total		25191662	533899				

The enantioseparation of **PCN 1515 (cross)** was eluting with hexane/dichloromethane (98/2, V/V) at flow rates of 3.0 mL/min using a CHIRALPAK IF[®] column (250 mm L × 10 mm I. D.). The first peak was an optically pure compound *R*_p-**PCN 1515**, and the second peak was *S*_p-**PCN 1515**. The last peak was an optically pure compound **PCN 1515 cross**. The normal loss of the instrument has been taken into account and does not affect subsequent experiments.

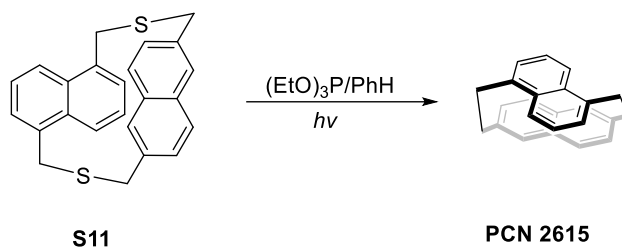
1.1.4. Synthesis and characterization of PCN 1526.

1.1.4.1. Synthesis of **S11**:



A solution of **S8** 156 mg (0.50 mmol) and **S4** 110 mg (0.50 mmol) in 40 ml dry THF was slowly added into a solution of THF (80 ml) containing *t*-BuOK in a nitrogen atmosphere under room temperature. The addition took 15 h. The solution was concentrated in vacuo, and the residue was chromatographed on silica gel with dichloromethane to give the desired product **S11** in the first eluate, 63 mg, yield: 34%, white solid.

1.1.4.2. Synthesis of **PCN 2615**:



S11 90 mg (0.24 mmol), triethyl phosphite 10 ml, and benzene 15 ml were placed in a quartz tube. The suspension was irradiated with a 6W UV lamp for 12 h in a nitrogen atmosphere. It was evaporated, and the residue was purified by high performance liquid chromatography to give the desired product **PCN 2615**, 16 mg (17%), white solid.

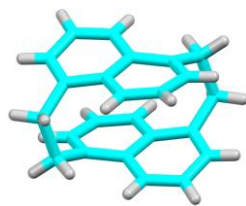


Table S1 Crystal data and structure refinement for PCN 1515.

Identification code	PCN 1515
Empirical formula	$C_{24}H_{20}$
Formula weight	308.40
Temperature/K	292.63(10)
Crystal system	monoclinic
Space group	$P2_1/c$
$a/\text{\AA}$	8.4113(2)
$b/\text{\AA}$	11.9596(2)
$c/\text{\AA}$	8.1538(2)
$\alpha/^\circ$	90
$\beta/^\circ$	105.735(3)
$\gamma/^\circ$	90
Volume/ \AA^3	789.50(3)
Z	2
$\rho_{\text{calc}}/\text{g/cm}^3$	1.297
μ/mm^{-1}	0.550
F(000)	328.0
Crystal size/ mm^3	$0.38 \times 0.26 \times 0.22$
Radiation	$\text{CuK}\alpha$ ($\lambda = 1.54184$)
2θ range for data collection/ $^\circ$	13.206 to 134.112
Index ranges	$-9 \leq h \leq 10, -13 \leq k \leq 14, -9 \leq l \leq 7$
Reflections collected	6680
Independent reflections	1392 [$R_{\text{int}} = 0.0338, R_{\text{sigma}} = 0.0262$]
Data/restraints/parameters	1392/0/109
Goodness-of-fit on F^2	1.059
Final R indexes [$I \geq 2\sigma(I)$]	$R_1 = 0.0388, wR_2 = 0.0966$
Final R indexes [all data]	$R_1 = 0.0429, wR_2 = 0.0988$
Largest diff. peak/hole / $e \text{\AA}^{-3}$	0.14/-0.13
Flack parameter	-0.2(10)



Table S2 Crystal data and structure refinement for R_p -PCN 1515 cross.

Identification code	R_p -PCN 1515 cross
Empirical formula	$C_{24}H_{20}$
Formula weight	308.40
Temperature/K	295.26(10)
Crystal system	orthorhombic
Space group	$P2_12_12_1$
$a/\text{\AA}$	8.4012(4)
$b/\text{\AA}$	13.0954(5)
$c/\text{\AA}$	15.0942(6)
$\alpha/^\circ$	90
$\beta/^\circ$	90
$\gamma/^\circ$	90
Volume/ \AA^3	1660.62(12)
Z	4
$\rho_{\text{calc}}/\text{g/cm}^3$	1.234
μ/mm^{-1}	0.523
F(000)	656.0
Crystal size/ mm^3	$0.36 \times 0.32 \times 0.26$
Radiation	$\text{CuK}\alpha$ ($\lambda = 1.54184$)
2Θ range for data collection/ $^\circ$	12.056 to 134.144
Index ranges	$-9 \leq h \leq 9, -15 \leq k \leq 15, -18 \leq l \leq 18$
Reflections collected	37202
Independent reflections	2938 [$R_{\text{int}} = 0.1103, R_{\text{sigma}} = 0.0559$]
Data/restraints/parameters	2938/0/218
Goodness-of-fit on F^2	1.057
Final R indexes [$I \geq 2\sigma(I)$]	$R_1 = 0.0450, wR_2 = 0.1126$
Final R indexes [all data]	$R_1 = 0.0543, wR_2 = 0.1193$
Largest diff. peak/hole / $e \text{\AA}^{-3}$	0.12/-0.14
Flack parameter	-0.2(10)

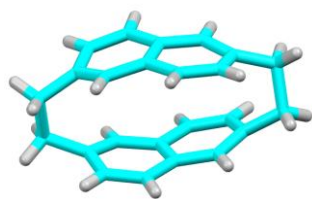


Table S3 Crystal data and structure refinement for *S_p*-PCN 2626.

Identification code	<i>S_p</i> -PCN 2626
Empirical formula	C ₂₄ H ₂₀
Formula weight	308.40
Temperature/K	295.26(10)
Crystal system	monoclinic
Space group	P2 ₁
a/Å	8.4807(3)
b/Å	8.4592(3)
c/Å	11.4471(4)
α/°	90
β/°	96.815(3)
γ/°	90
Volume/Å ³	815.41(5)
Z	2
ρ _{calc} /cm ³	1.256
μ/mm ⁻¹	0.532
F(000)	328.0
Crystal size/mm ³	0.32 × 0.28 × 0.22
Radiation	CuKα (λ = 1.54184)
2θ range for data collection/°	7.778 to 134.13
Index ranges	-10 ≤ h ≤ 10, -10 ≤ k ≤ 9, -13 ≤ l ≤ 13
Reflections collected	15203
Independent reflections	2662 [R _{int} = 0.0444, R _{sigma} = 0.0250]
Data/restraints/parameters	2662/1/218
Goodness-of-fit on F ²	1.124
Final R indexes [I ≥ 2σ (I)]	R ₁ = 0.1071, wR ₂ = 0.2983
Final R indexes [all data]	R ₁ = 0.1073, wR ₂ = 0.2985
Largest diff. peak/hole / e Å ⁻³	0.60/-0.37
Flack parameter	0.0(10)



Table S4. Crystal data and structure refinement for *S_p*-PCN 2615.

Identification code	<i>S_p</i> -PCN 2615	
Empirical formula	C ₂₄ H ₂₀	
Formula weight	308.40	
Temperature	293(1) K	
Wavelength	1.54178 Å	
Crystal system	Tetragonal	
Space group	P4 ₃ 2 ₁ 2	
Unit cell dimensions	a = 8.9248(3) Å	α = 90°.
	b = 8.9248(3) Å	β = 90°.
	c = 20.831(2) Å	γ = 90°.
Volume	1659.26(19) Å ³	
Z	4	
Density (calculated)	1.235 Mg/m ³	
Absorption coefficient	0.523 mm ⁻¹	
F(000)	656	
Crystal size	0.2 x 0.1 x 0.1 mm ³	
Theta range for data collection	5.392 to 76.223°.	
Index ranges	-10 ≤ h ≤ 8, -11 ≤ k ≤ 9, -25 ≤ l ≤ 26	
Reflections collected	18939	
Independent reflections	1695 [R(int) = 0.0837]	
Completeness to theta = 67.679°	100.0 %	
Absorption correction	Semi-empirical from equivalents	
Max. and min. transmission	1.00000 and 0.60837	
Refinement method	Full-matrix least-squares on F ²	
Data / restraints / parameters	1695 / 330 / 218	
Goodness-of-fit on F ²	1.076	
Final R indices [I > 2σ(I)]	R1 = 0.0547, wR2 = 0.1646	
R indices (all data)	R1 = 0.0739, wR2 = 0.1878	
Absolute structure parameter	-1.0(10)	
Extinction coefficient	n/a	
Largest diff. peak and hole	0.076 and -0.095 e.Å ⁻³	

1.2. Transient absorption spectroscopy

Comprehensive details on nanosecond time-resolved transient absorbance instrumentation can be found in previous studies. Briefly summarizing, the regenerative amplifier (Astrella, Coherent Inc.) is seeded by the Ti:Sapphire oscillator (Viatra, Coherent Inc.). This setup enables the amplifier to produce a 7 mJ 90 femtosecond (fs) pulse train at a central wavelength of 800 nm with a repetition rate of 1 kHz. Following amplification, a beam splitter is set to divide these pulses into two beam paths. One of them is assigned to a pump-optical parametric amplifier (OPerA Solo, Coherent Inc.). OPerA is tuned to produce light with a specific wavelength that works as a pump beam. At the same time, the probe beam is generated by triggering a photon diode with an electronic signal and overlapped with the pump beam in a fused silica cell with a path length of 2 millimeters. Furthermore, a magnetic stirring rod was used to maintain the homogeneity of solutions during laser experiments. Finally, nanosecond time-resolved transient absorption spectra were measured by TA spectrometer (Helios-EOS ultrafast System). The Glotaran program version 1.5.1³ was used to analyze the TA data and the decay-associated difference spectra (DADS) was obtained from this program.

1.3. Steady-State UV/Vis Absorption

The steady-state UV/vis absorption spectra were measured by using a dual-beam UV–vis spectrometer (TU1901, Beijing Purkinje General Instrument Co. Ltd.). The background noise and solvent signal were subtracted for all steady-state UV/vis absorption spectra.

1.4. Triplet quantum yield calculation

Triplet quantum yield of 1515, 2615, 2626 and 1515_{cross} dichloromethane solution were calculated by TA spectra excited at 285 nm. The formula for calculating the initial singlet excited state concentration is:

$$[S^*] = \frac{(\text{photos/pulse})(1 - I/I_0)}{N_A V}$$

where the number of photons per excitation pulse (285 nm) is:

$$\frac{\text{photos}}{\text{pulse}} = \frac{\text{power}}{(\text{rep rate})(\text{energy per photo})}$$

For example, as for 1515, the number of photons per excitation pulse is:

$$= \frac{5.0 \times 10^{-4} \text{ J s}^{-1}}{1000 \text{ s}^{-1} \times \frac{1240}{285} \times 1.6 \times 10^{-19} \text{ J}} = 7.18 \times 10^{11}$$

and $V = A_{red} \times d = \pi \times (3.85 \times 10^{-3} \text{ dm})^2 \times 0.02 \text{ dm} = 9.30 \times 10^{-7} \text{ L}$

So the initial singlet excited concentration of 1515 is:

$$[S_{1515}^*] = \frac{(\text{photos/pulse})(1 - I/I_0)}{N_A V} = 1.27 \times 10^{-6} \text{ mol/L}$$

Similarly, the initial singlet excited concentration of 2615, 2626 and 1515_{cross} is:

$$[S_{2615}^*] = \frac{(\text{photos/pulse})(1 - I/I_0)}{N_A V} = 1.76 \times 10^{-6} \text{ mol/L}$$

$$[S_{2626}^*] = \frac{(\text{photos/pulse})(1 - I/I_0)}{N_A V} = 1.27 \times 10^{-6} \text{ mol/L}$$

$$[S_{1515\text{cross}}^*] = \frac{(\text{photos/pulse})(1 - I/I_0)}{N_A V} = 1.24 \times 10^{-6} \text{ mol/L}$$

The average intensity of the specific ESA signal at 430 nm which is assigned to the triplet state can be obtained from decay-associated difference spectra (DADS) after excited at 285 nm. And the triplet extinction coefficient of the compound is known from the triplet sensitization experiments.⁴ So the triplet excited state concentration can be calculated as:

$$[T_{1515}^*] = \frac{\Delta A}{\epsilon^T (430 \text{ nm}) \times l} = \frac{1.7 \times 10^{-3}}{7600 \times 0.2} = 1.12 \times 10^{-6} \text{ mol/L}$$

$$[T_{2615}^*] = \frac{\Delta A}{\epsilon^T (430 \text{ nm}) \times l} = \frac{1.9 \times 10^{-3}}{7600 \times 0.2} = 1.25 \times 10^{-6} \text{ mol/L}$$

$$[T_{2626}^*] = \frac{\Delta A}{\epsilon^T (430 \text{ nm}) \times l} = \frac{1.5 \times 10^{-3}}{7600 \times 0.2} = 9.87 \times 10^{-7} \text{ mol/L}$$

$$[T_{1515\text{cross}}^*] = \frac{\Delta A}{\epsilon^T (430 \text{ nm}) \times l} = \frac{1.0 \times 10^{-3}}{7600 \times 0.2} = 6.58 \times 10^{-7} \text{ mol/L}$$

So the triplet quantum yield of compound in dichloromethane solution is:

$$1515: \phi_T = \frac{[T_{\text{urd}}^*]}{[S_{\text{urd}}^*]} = 88.1\% \quad 2615: \phi_T = \frac{[T_{\text{urd}}^*]}{[S_{\text{urd}}^*]} = 71.0\%$$

$$2626: \phi_T = \frac{[T_{\text{urd}}^*]}{[S_{\text{urd}}^*]} = 77.7\% \quad 1515_{\text{cross}}: \phi_T = \frac{[T_{\text{urd}}^*]}{[S_{\text{urd}}^*]} = 53.1\%$$

2. Additional experimental results

2.1. DCM experiments

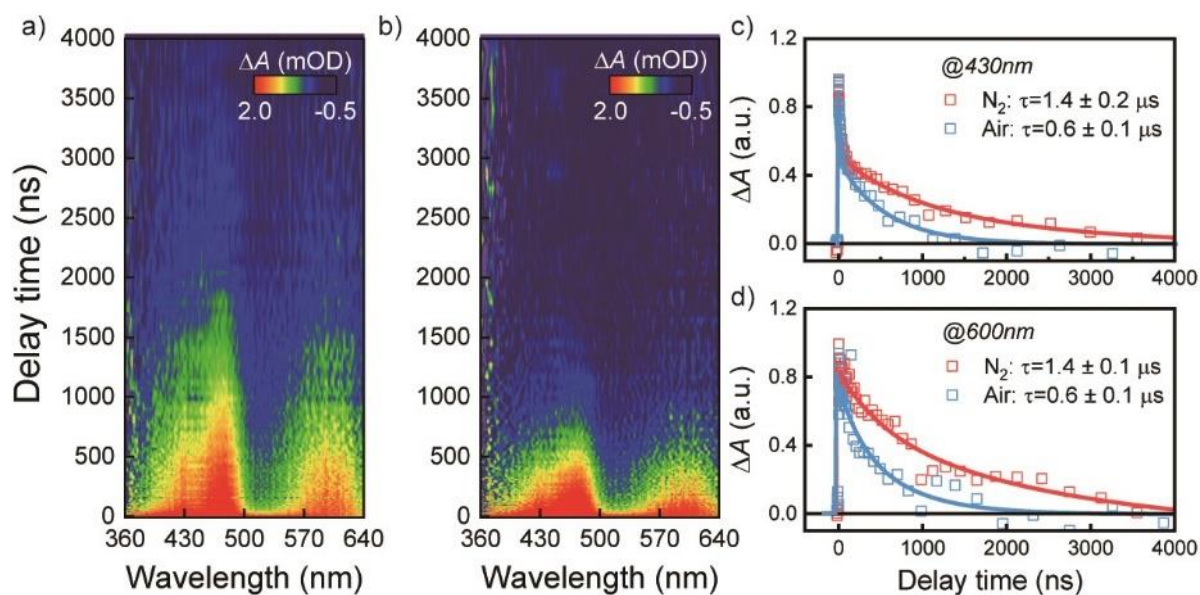


Figure S1. Nanosecond transient absorption spectra of 1515 under (a) N_2 -saturated and (b) air conditions. Back-to-back normalized kinetic traces of 1515 probed at (c) 430 nm and (d) 600 nm.

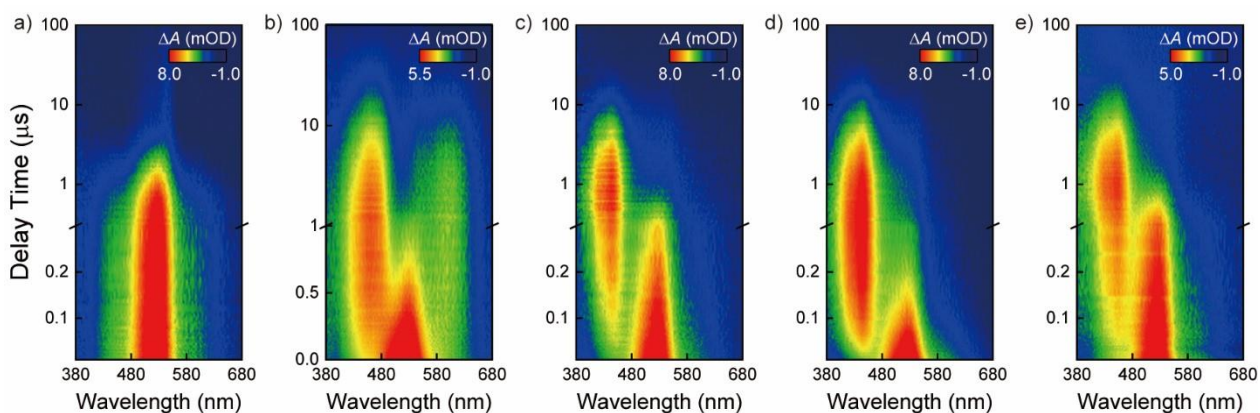


Figure S2. (a) Nanosecond transient absorption spectra of triplet sensitizer benzophenone excited at 355 nm under N_2 -saturated conditions. (b-e) Nanosecond transient absorption spectra for triplet sensitization experiments of 1515, 2615, 2626 and 1515_{cross} excited at 355 nm under N_2 -saturated conditions.

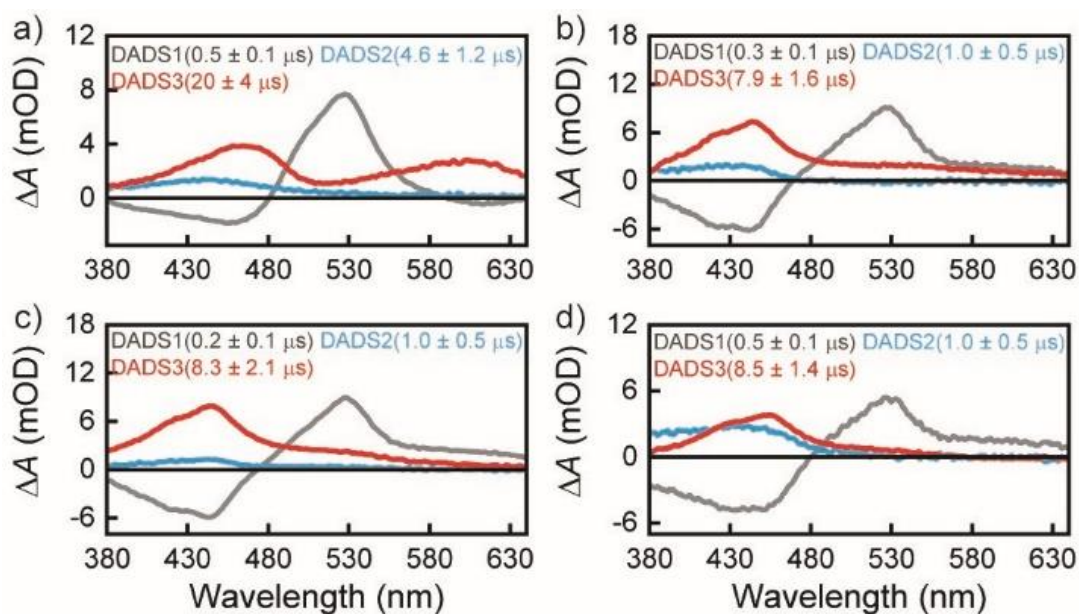


Figure S3. Decay-associated difference spectra (DADS) of triplet sensitization experiments of (a) 1515, (b) 2615, (c) 2626 and (d) 1515_{cross} excited at 355 nm under N₂-saturated conditions.

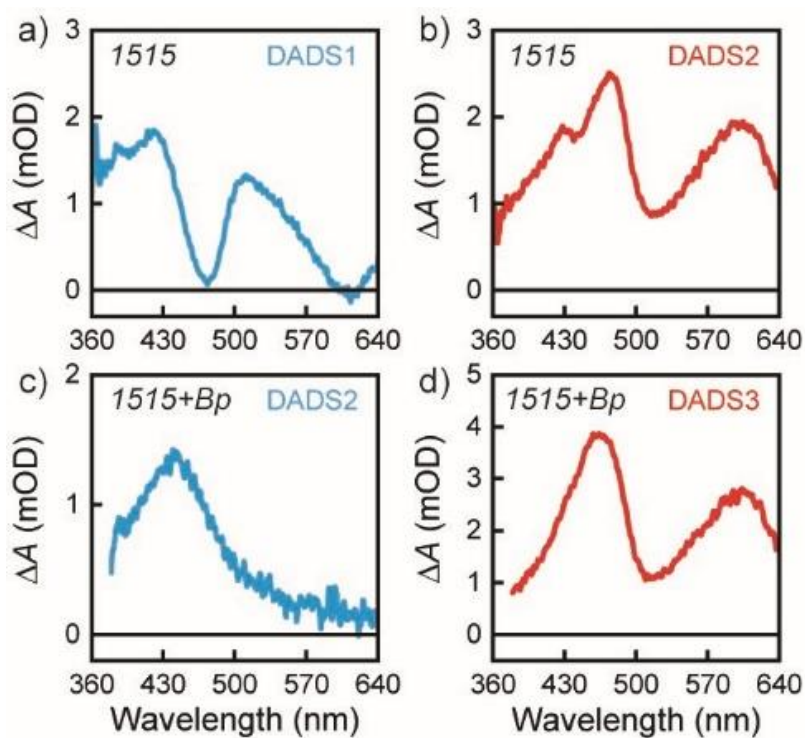


Figure S4. Comparison of decay-associated difference spectra (DADS) between (a, b) direct excitation and (c, d) sensitization experiments of 1515.

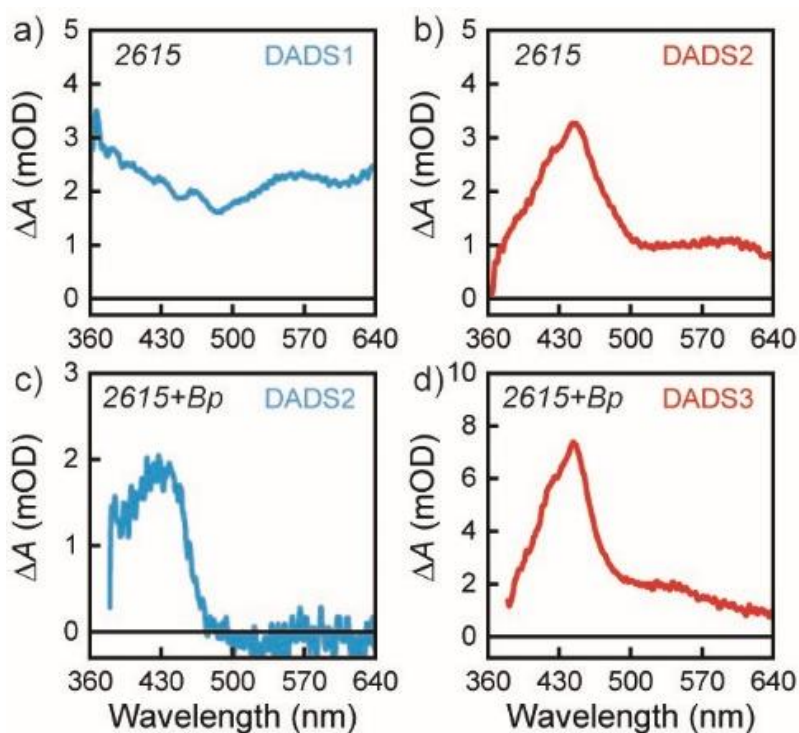


Figure S5. Comparison of decay-associated difference spectra (DADS) between (a, b) direct excitation and (c, d) sensitization experiments of 2615.

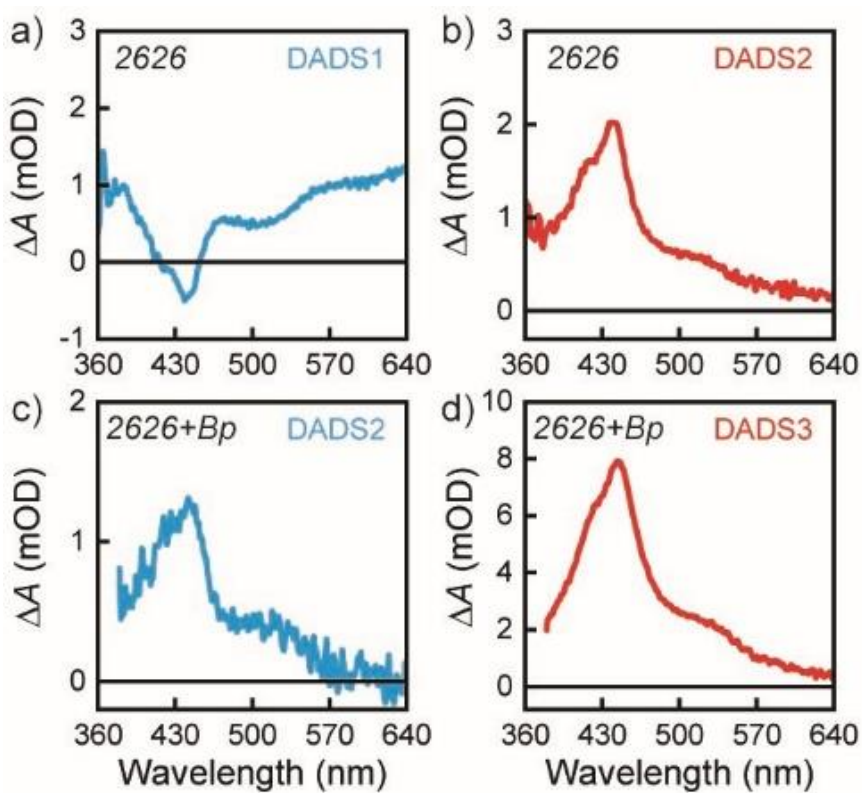


Figure S6. Comparison of decay-associated difference spectra (DADS) between (a, b) direct excitation and (c, d) sensitization experiments of 2626.

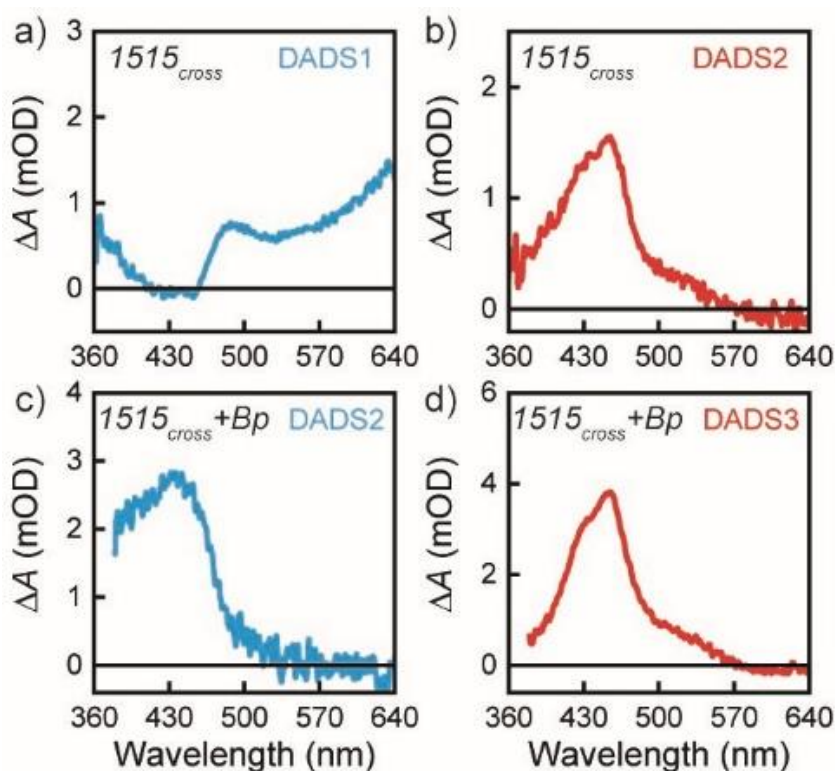


Figure S7. Comparison of decay-associated difference spectra (DADS) between (a, b) direct excitation and (c, d) sensitization experiments of 1515_{cross} .

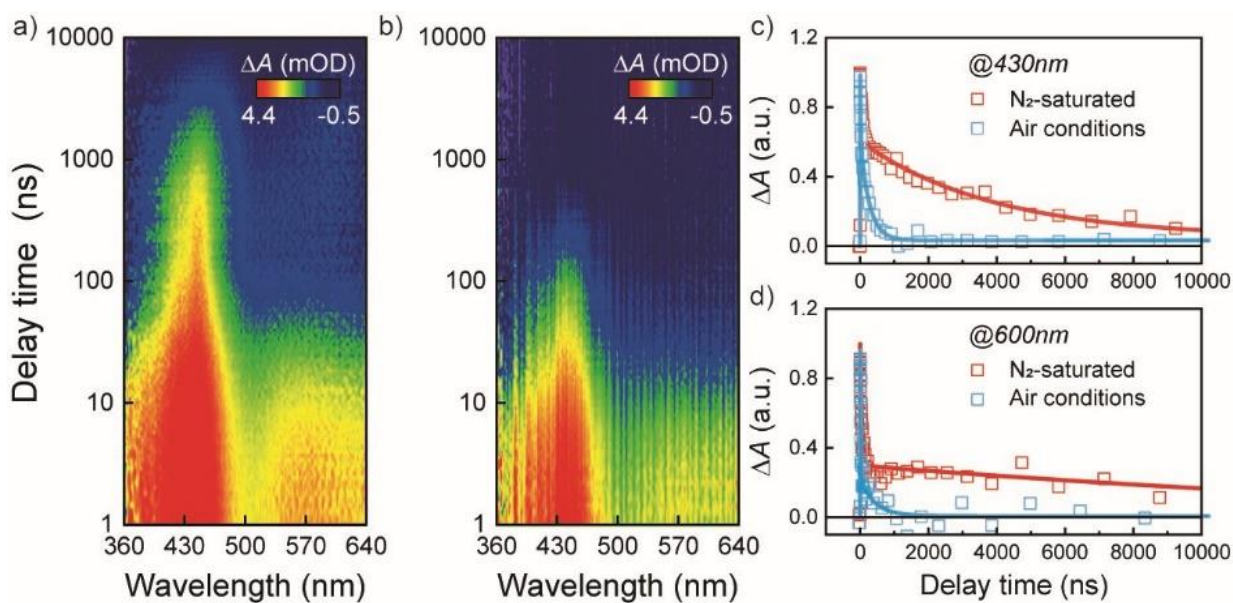


Figure S8. Nanosecond transient absorption spectra of 2615 under (a) N_2 -saturated and (b) air conditions. Back-to-back normalized kinetic traces of 2615 probed at (c) 430 nm and (d) 600 nm.

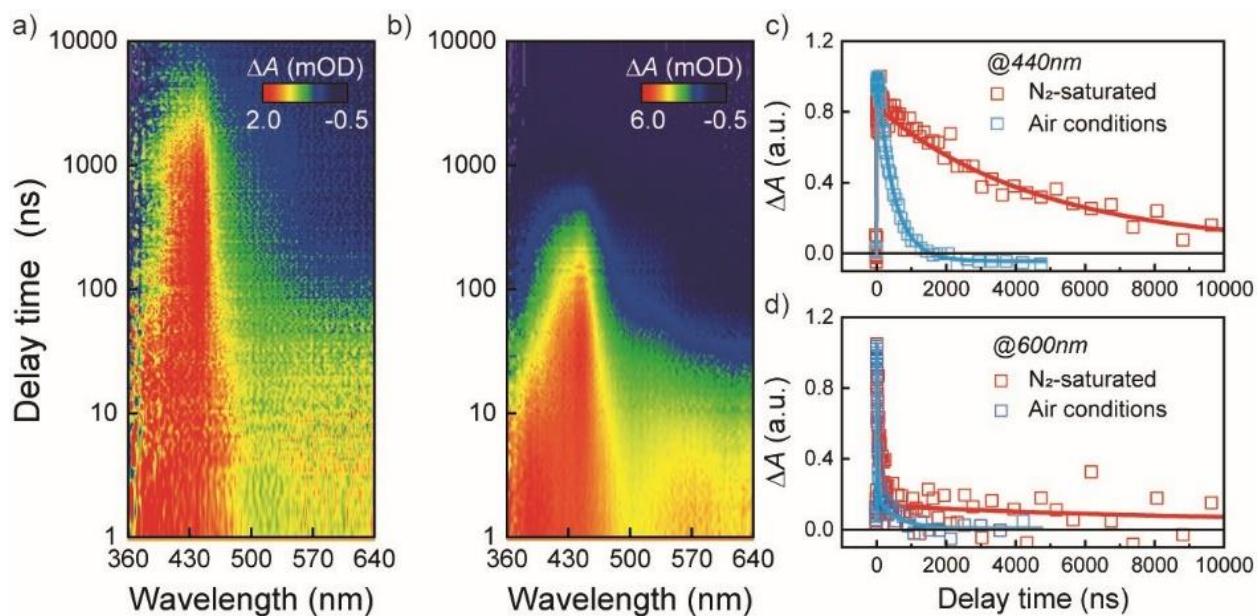


Figure S9. Nanosecond transient absorption spectra of 2626 under (a) N_2 -saturated and (b) air conditions. Back-to-back normalized kinetic traces of 2626 probed at (c) 440 nm and (d) 600 nm.

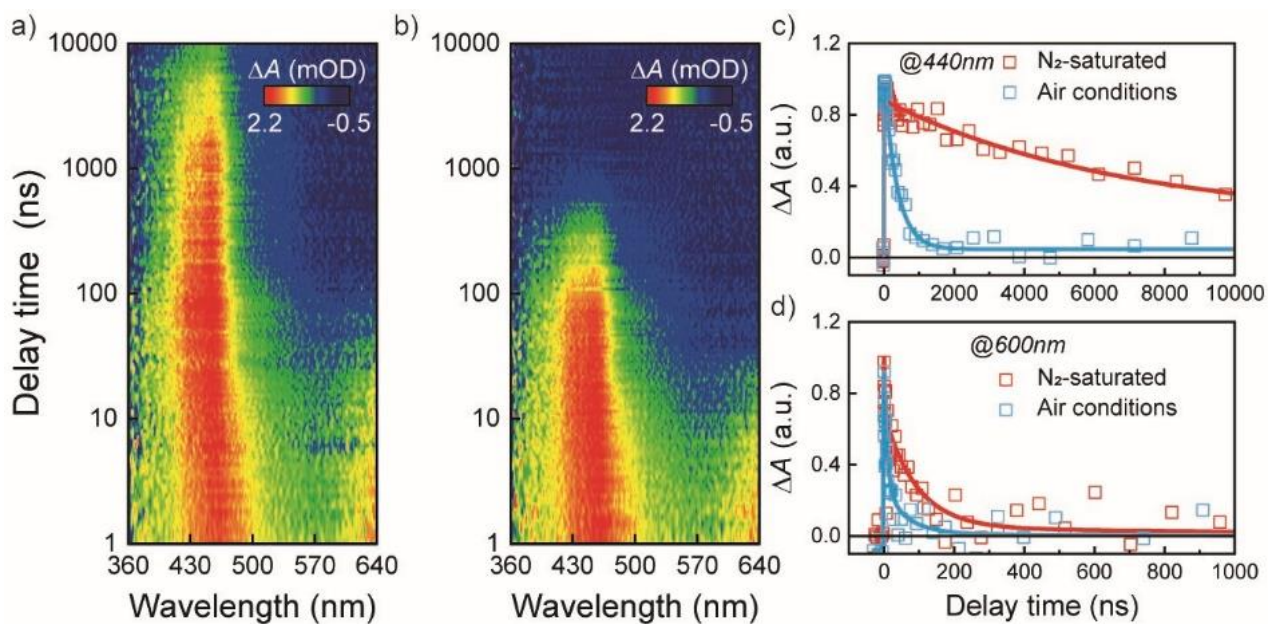


Figure S10. Nanosecond transient absorption spectra of 1515_{cross} under (a) N_2 -saturated and (b) air conditions. Back-to-back normalized kinetic traces of 1515_{cross} probed at (c) 440 nm and (d) 600 nm.

Table S5. Triplet quantum yield of all the samples in dichloromethane excited at 285 nm

Compound	Triplet quantum yield
1515	88.1%
2615	71.0%
2626	77.7%
1515 _{cross}	53.1%

2.2. ACN experiments

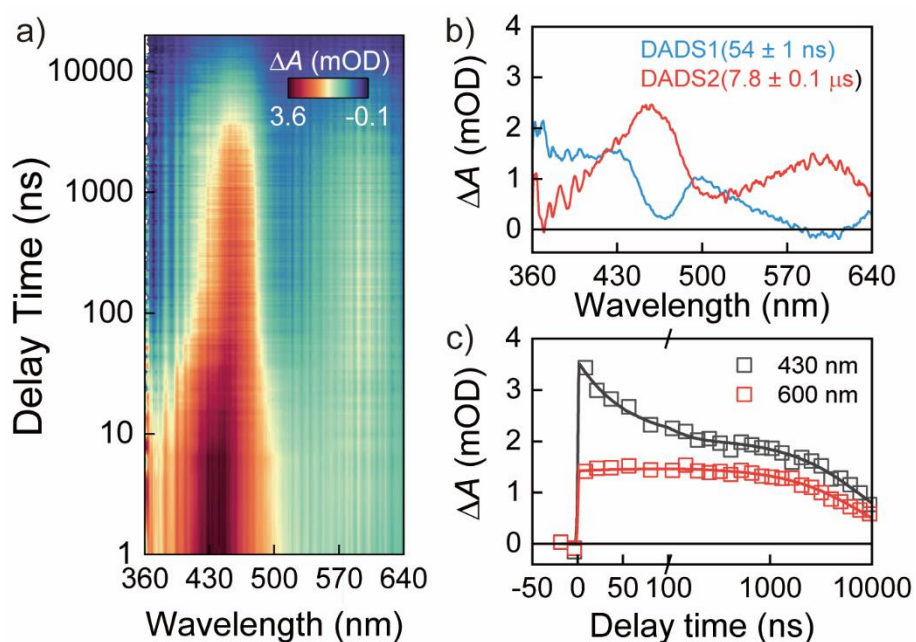


Figure S11. (a) Nanosecond time-resolved transient absorption spectra of 1515 in acetonitrile excited at 285 nm. (b) Decay-associated difference spectra (DADS) and (c) kinetic traces probed at 430 nm and 600 nm.

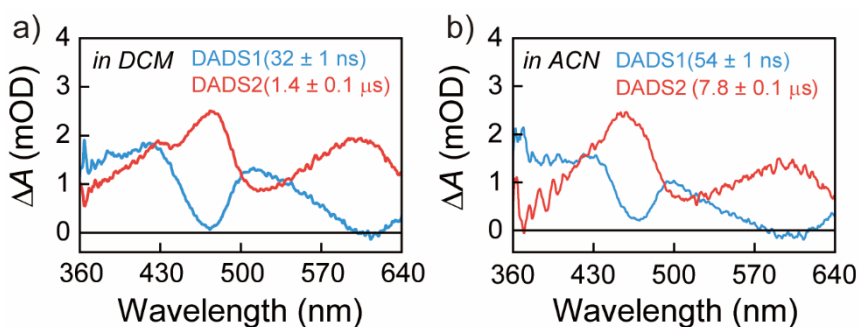


Figure S12. DADS for 1515 in dichloromethane and acetonitrile (ACN).

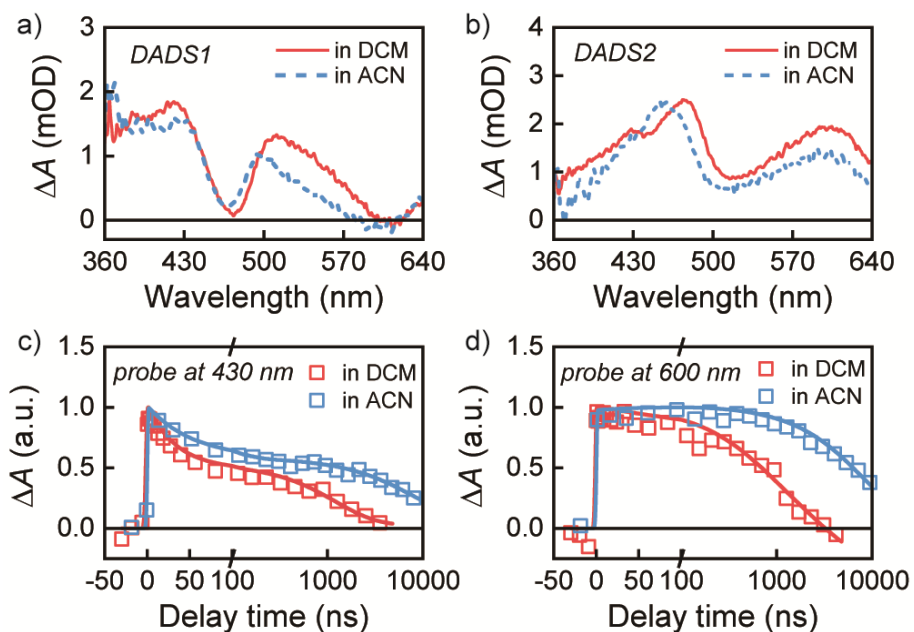


Figure S13. (a, b) Comparison of DADS for 1515 in acetonitrile and dichloromethane. (c, d) Comparison of kinetic traces for 1515 in acetonitrile and dichloromethane probe at 430 nm and 600 nm.

The TA spectrum of achiral 1515 in acetonitrile is similar to the one reported in dichloromethane in the main text, with ESA signals present at 425 nm, 475 nm, and 600 nm. And the DADS spectra obtained through global fitting are also consistent in shape, as shown in Figure S12 and Figure S13. The difference is that the excited-state lifetime in acetonitrile is significantly longer, yielding lifetimes of 54 ± 1 ns and 7.8 ± 0.1 μ s.

3. Computational methods

-Electronic calculations. We resorted to Density Functional Theory (DFT) calculations, adopting both standard density functionals, as M052X⁵ and ω B97XD⁶, which has been already profitably adopted to study closely stacked systems, and double hybrid B2PLYPD3^{7,8} functionals. Double hybrid functionals recently emerged as very promising tools for the calculation of the excited state properties of several class of compounds, as acenes, that are instead problematic for many standard density functionals.⁹⁻¹¹ The spectra have been computed both at the TD level and both by using Tamm-Dancoff approximation (TDA), which, in many systems, has been shown to provide a more balanced treatment of singlet and triplet excited states.

-Solvent effects have been included by the implicit Polarizable Continuum Method (PCM).^{12, 13}

-Spectra simulations. The absorption spectra of the dimers have been simulated by broadening the stick transitions with a phenomenological gaussian with half width half maximum =0.2 eV. In a parallel study, we checked that, when applied to the monomer, this procedure provides spectral lineshape in good agreement with the reference computed with FCClasses3.¹⁴

The calculations have been performed using the Gaussian16¹⁵ and Orca 5.0¹⁶ quantum chemistry codes.

4. Additional computational results

4.1. Stabilities

Table S6. Relative energy (in eV), with respect to T₁-exc-min, of T₁-loc-min located for the dinaphthalene compounds here studied, in the gas phase or in DCM solution. Electronic energy in black, free energy in red.

species	Gas Phase		DCM	
	B2PLYPD3 6-31+G(d,p)	ωB97XD 6-31+G(d,p)	M052X 6-31+G(d,p)	M052X aug-cc-pvtz
1515	-0.02	-0.45 -0.55	-0.367 -0.442	-0.354 -0.460
2626	-0.22	-0.65 -0.74	-0.567 -0.657	-0.547 -0.634
2615	-0.07	-0.49 -0.61	-0.397 ^a -0.517	0.392 -0.522
1515 _{cross}	-0.21	-0.66 -0.74	-0.567 -0.661	

a) Other localized triplet: M052X: -0.384 -0.562; ωB97XD: -0.473 -0.626; B2BLYPD3: -0.046 -0.136; b)
cc-pvtz level: 1515: +0.005 ; 2626: -0.189; 2615 -0.049; 1515_{cross} :

4.2. Geometrical parameters

Table S7. Main geometrical parameters (in Å or in °) of the lowest energy singlet and triplet minima for 15dimethyl naphthalene and 1515 dimer. See Scheme 1 in the main text and Figure S8 for the definition of the geometrical parameter. B2LYPD3/6-31+G(d,p) calculations

	monomer		1515			
	S ₀	T ₁	T ₁ -exc-min		T ₁ -loc-min	
			mon1	mon2	triplet	Singlet
r _i	1.435	1.447	1.44	1.44	1.450	1.435
r _o	1.41	1.37	1.39	1.39	1.37	1.41
r _{im}	1.43/1.42 ^a	1.43/1.41 ^a	1.43/1.42 ^a	1.43/1.42 ^a	1.43/1.40 ^a	1.43/1.42 ^a
r _{om}	1.38/1.38 ^a	1.44/1.44 ^a	1.41/1.41 ^a	1.43/1.42 ^a	1.44/1.43 ^a	1.39/1.38 ^a
d			3.0		3.13	
η			-3.0		-12.2	

a) the first value concerns the bond bearing the methyl substituent, average over the two bonds

Table S8. Main geometrical parameters (in Å or in °) of the lowest energy singlet and triplet minima for 26dimethyl naphthalene and 2626 dimer. See Scheme 1 in the main text and Figure S8 for the definition of the geometrical parameter. B2LYPD3/6-31+G(d,p) calculations

	monomer		2626			
	S ₀	T ₁	T ₁ -exc-min		T ₁ -loc-min	
			mon1	mon2	triplet	Singlet
r _i	1.429	1.443				
r _o	1.42	1.37				
r _{im}	1.42	1.41				
r _{om}	1.38	1.44				
d						
η						

Table S9. Main geometrical parameters (in Å or in °) of the triplet minima for 1515, 2626, 2615 and 1515_{cross}. PCM/ ω B97XD/6-31+G(d,p) calculations.

	1515				2626			
	T ₁ -exc-min		T ₁ -loc-min		T ₁ -exc-min		T ₁ -loc-min	
	mon1	mon2	triplet	Singlet	mon1	mon2	triplet	Singlet
r _i	1.44	1.44	1.45	1.42	1.44	1.44	1.45	1.42
r _o	1.38	1.38	1.36	1.41	1.40	1.40	1.37	1.42
d	3.0		3.2		3.34		3.48	
η	-2.8		-13.3		16.0		-39.2	
	2615				1515 _{cross}			
	T ₁ -exc-min		T ₁ -loc-min		T ₁ -exc-min		T ₁ -loc-min	
	26-mon	15-mon	triplet	Singlet	mon1	mon2	triplet	Singlet
r _i	1.43	1.45	1.47	1.42	1.44	1.44	1.46	1.42
r _o	1.39	1.38	1.36	1.42	1.39	1.39	1.36	1.41
d	3.24		3.50		3.04		3.10	
η	-89.0		-79.6		-38.5		-51.7	

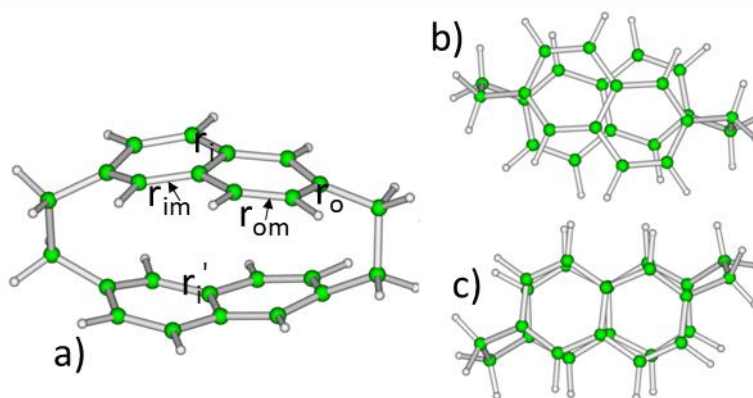


Figure S14. a) Schematic drawing of 2626, including the labelling for some geometrical parameters. b) top view of the most stable conformer c) top view of the f2f 2626 conformer.

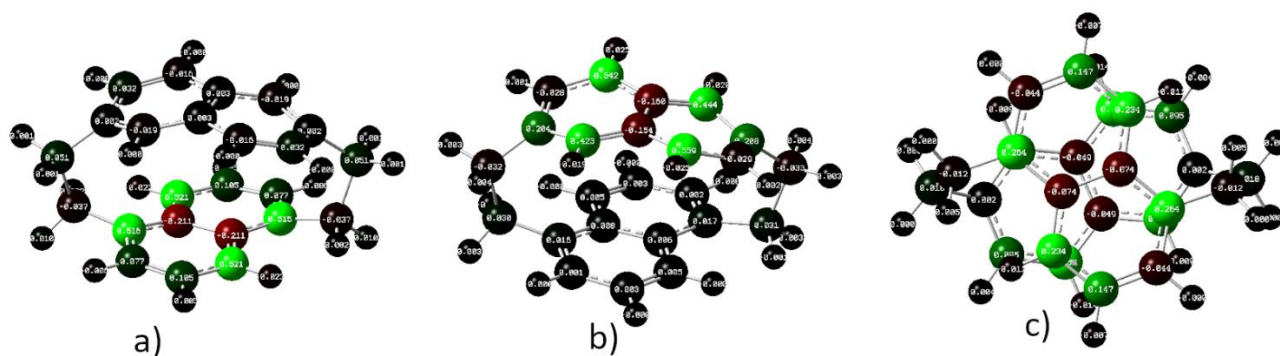


Figure S15. Mulliken spin population analysis for the three triplet minima located for 2615. a) T_1 -loc-min. b) T_1 -loc1-min. c) T_1 -exc-min. Color code. Positive spin density, green; negative spin density, red; Spin density close to 0, black. The values are written in white.

4.3. Additional spectra

4.3.1. 1515

4.3.1.1. In the Gas phase

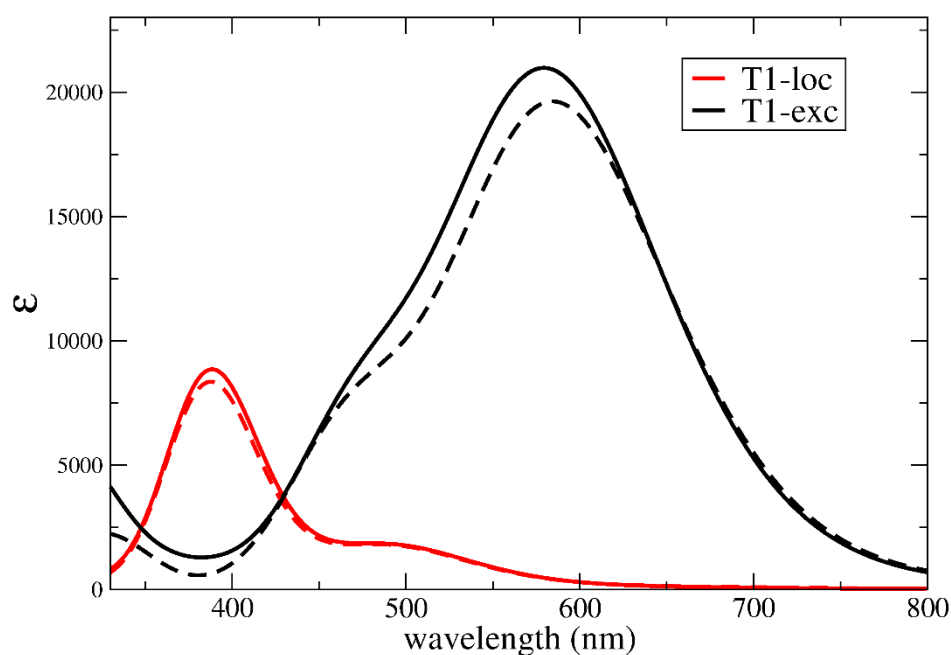


Figure S16. TDA Absorption spectra computed in the gas phase for the 1515 triplet minima located. T_1 -loc-min (red line), T_1 -exc-min (black line) in the gas phase. ω B97XD calculations with 6-31+G(d,p) (continuous lines) or def2TZVP (dashed lines) basis sets. Spectra simulated by broadening each stick transition with a gaussian with hwhm=0.25 eV .

4.3.1.2. In DCM

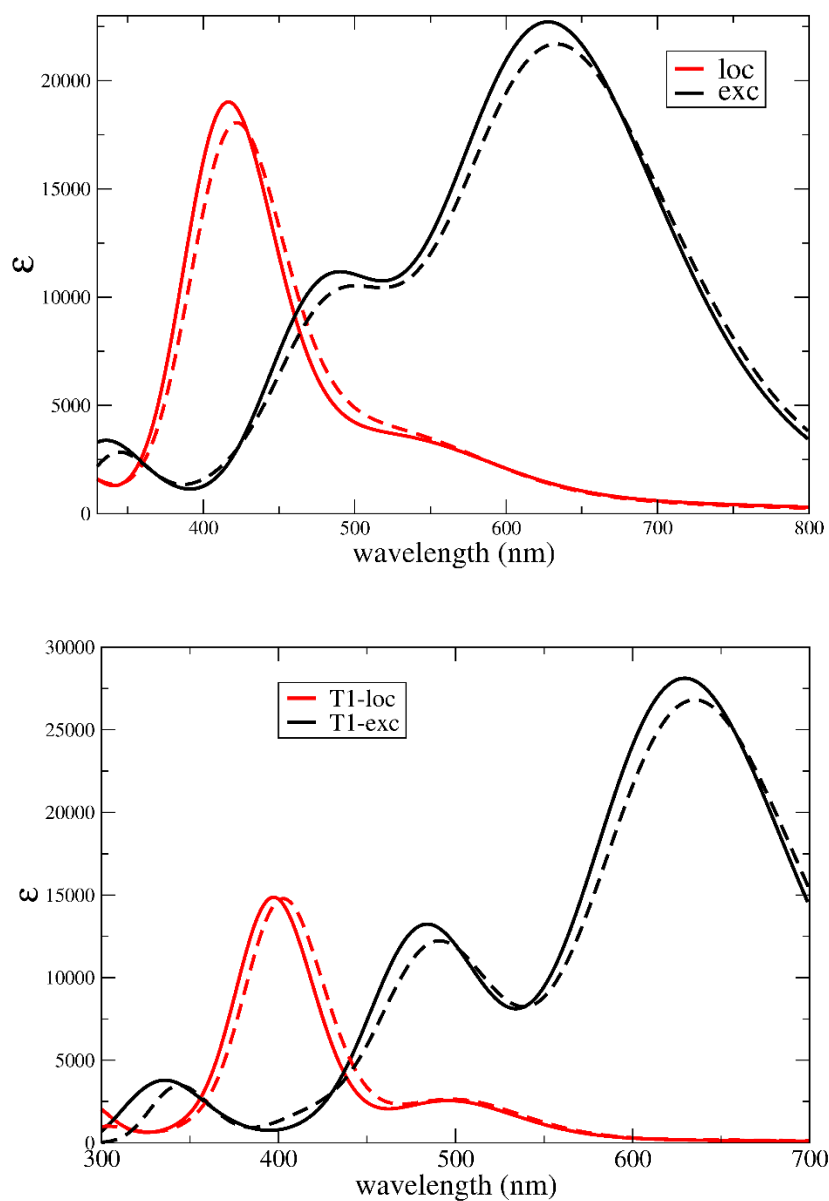


Figure S17. TDA Absorption spectra computed for the 1515 triplet minima located, T_1 -loc-min (red) and T_1 -exc-min (black) in DCM. PCM/ ω B97XD calculations with 6-31+G(d,p) (continuous lines) or aug-cc-pvtz (dashed lines). Spectra simulated by broadening each stick transition with a gaussian with hwhm=0.25 eV (upper panel) or 0.20 eV (lower panel)

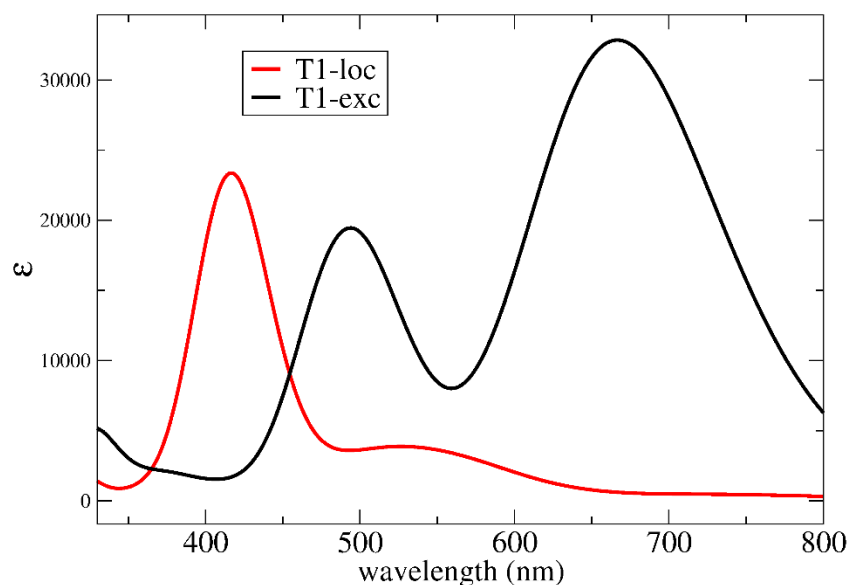


Figure S18. TDA Absorption spectra computed for the 1515 triplet minima located, T_1 -loc-min (red) and T_1 -exc-min (black) in DCM. PCM/M052X/6-31+G(d,p) calculations Spectra simulated by broadening each stick transition with a gaussian with 0.20 eV

4.3.2. 2626, 2615, 1515cross

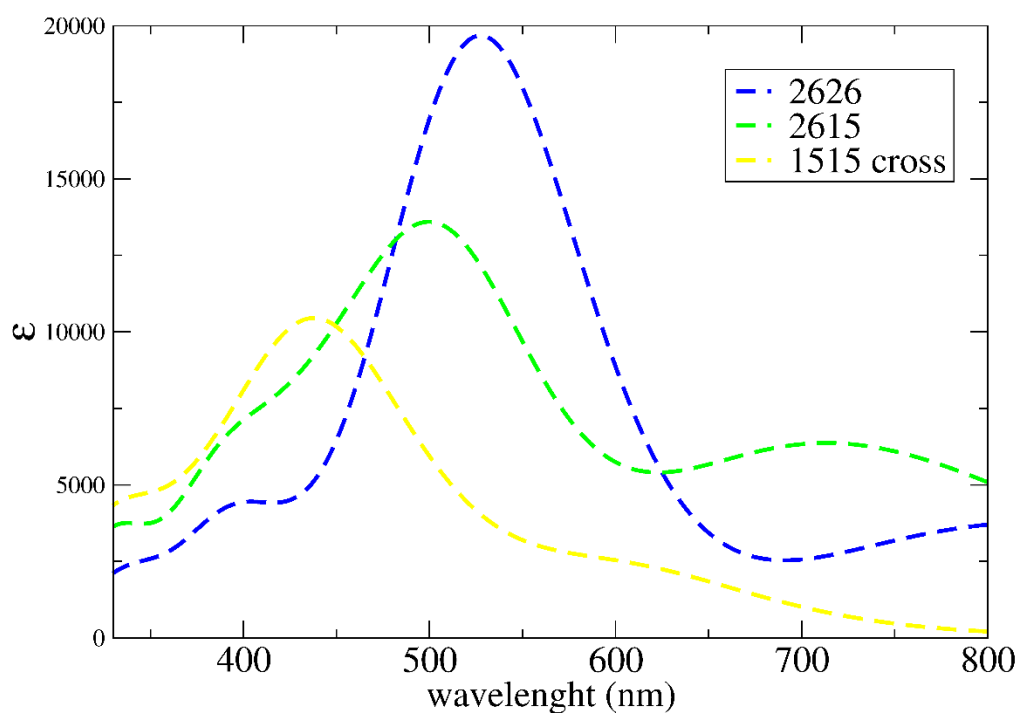


Figure S19. TDA Absorption spectra computed in the gas phase for the excimer minima located for 2626 (blue), 2615 (green) and 1515_{cross} (yellow). B2PLYPD3 calculations with the 6-31+G(d,p) basis set. Spectra simulated by broadening each stick transition with a gaussian with hwhm=0.25 eV

4.3.2.1. 2626

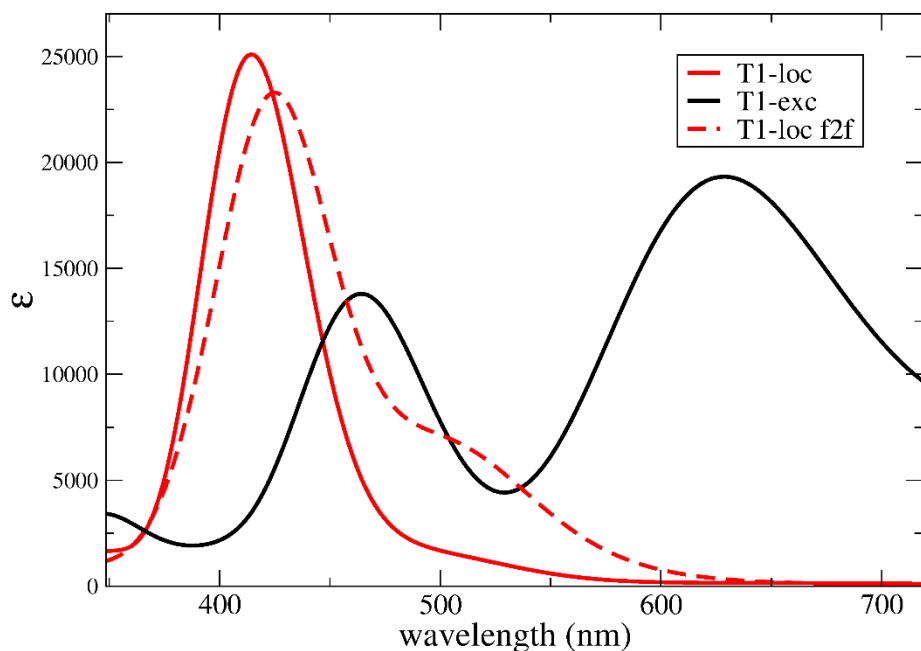


Figure S20. TDA Absorption spectra computed for the 2626 triplet minima located. T_1 -loc-min (black continuous line), T_1 -loc-f2f (dashed black line). T_1 -exc-min (red) in DCM. PCM/ ω B97XD/6-31+G(d,p) calculations. Spectra simulated by broadening each stick transition with a gaussian with hwhm=0.2 eV

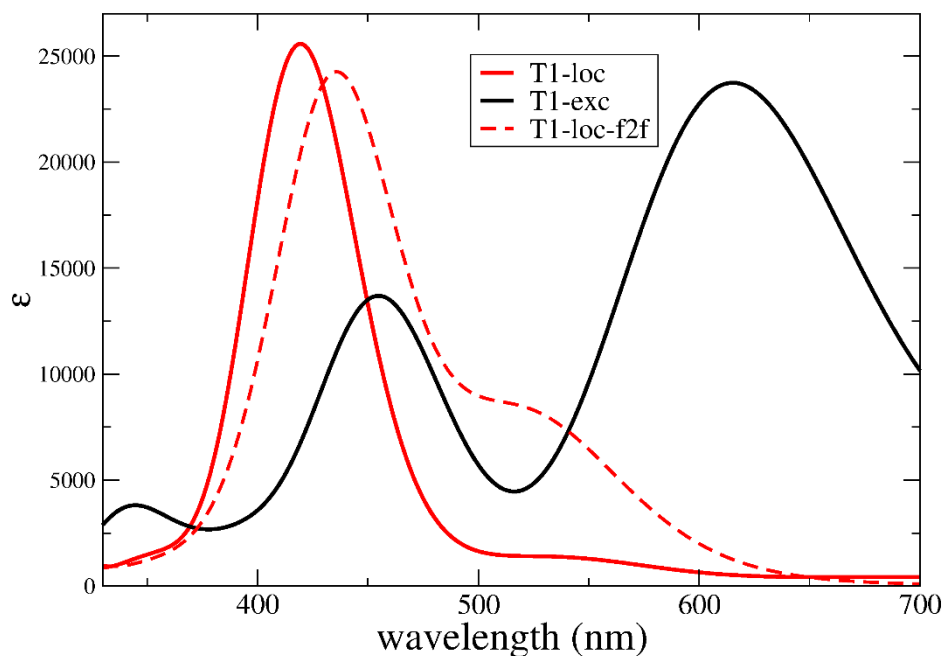


Figure S21. TDA Absorption spectra computed for the 2626 triplet minima located. T_1 -loc-min (black continuous line), T_1 -loc-f2f (dashed black line). T_1 -exc-min (red) in DCM. PCM/M052X/6-31+G(d,p) calculations. Spectra simulated by broadening each stick transition with a gaussian with hwhm=0.2 eV

The TDA absorption spectra computed for the triplet minima located for 2626 by PCM/ ω B97XD/6-31+G(d,p) calculations are reported in the Figures S12 above. T₁-loc and T₁-loc-f2f exhibit a strong absorption band at ~400 nm, with another shallow band (more intense for T₁-loc-f2f) above 500 nm. As found for 1515, two strong absorption bands peaking at ~500 and ~650 nm are present in the spectrum of T₁-exc. Based on the comparison **with the spectra reported in Figure 5, we can confirm the conclusions based on the B2LYPD3 spectra reported in the main text, i.e. that T₁-loc-min is the main responsible of long-living absorptions. In this case also, phosphorescence spectrum confirms our conclusion.**

4.3.2.2. 2615

As anticipated in the main text two different loc minima have been located for 2615, differing for the ring where the triplet is localized (see Figure S14 below)

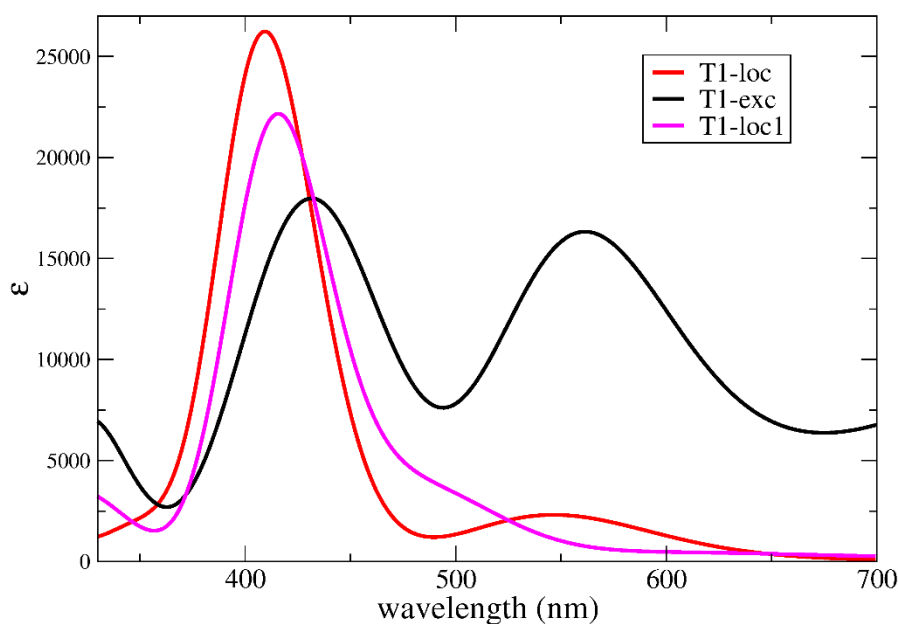


Figure S22. TDA Absorption spectra computed for the 2615 triplet minima located, T₁-loc-min (red) T₁-loc1-min (magenta) and T₁-exc-min (black) in DCM. PCM/ ω B97XD/6-31+G(d,p) calculations. Spectra simulated by broadening each stick transition with a gaussian with hwhm=0.2 eV

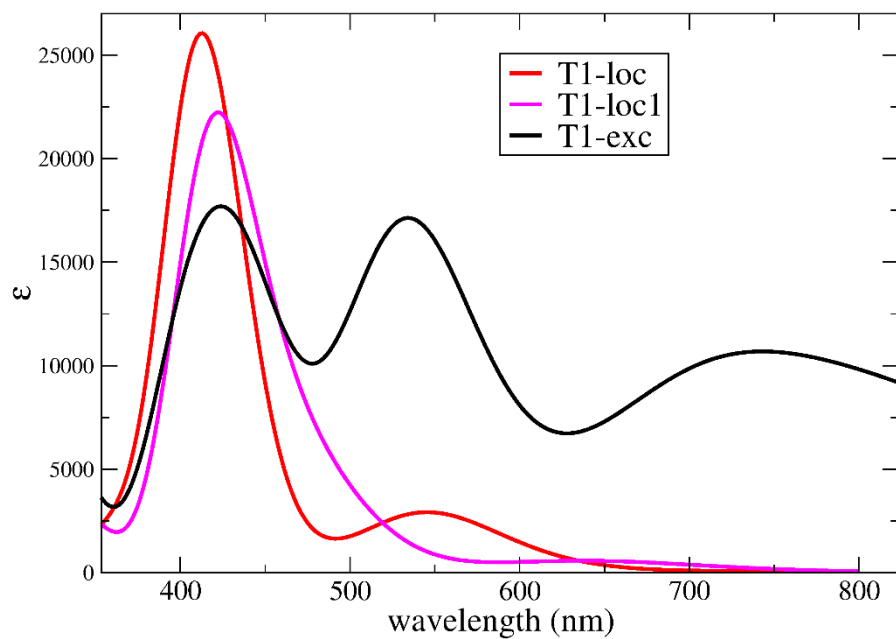


Figure S23. TDA Absorption spectra computed for the 2615 triplet minima located, T_1 -loc-min (red) T_1 -loc1-min (magenta) and T_1 -exc-min (black) in DCM. PCM/M052X/6-31+G(d,p) calculations. Spectra simulated by broadening each stick transition with a gaussian with hwhm=0.2 eV

4.3.2.3. 1515cross

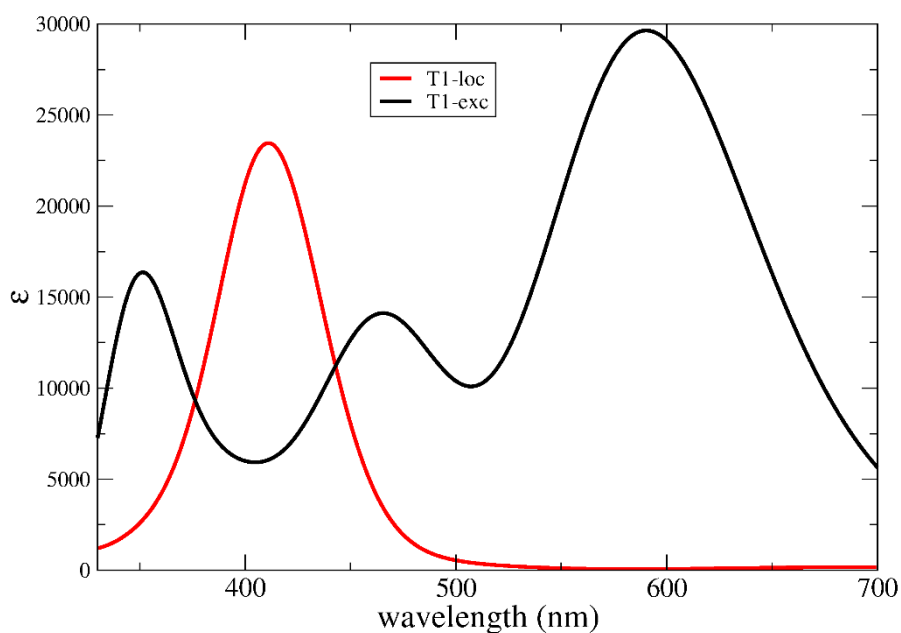


Figure S24. TDA Absorption spectra computed for the 1515_{perp} triplet minima located, T₁-loc-min (red) and T₁-exc-min (black) in DCM. PCM/ ω B97XD/6-31+G(d,p) calculations. Spectra simulated by broadening each stick transition with a gaussian with hwhm=0.2 eV

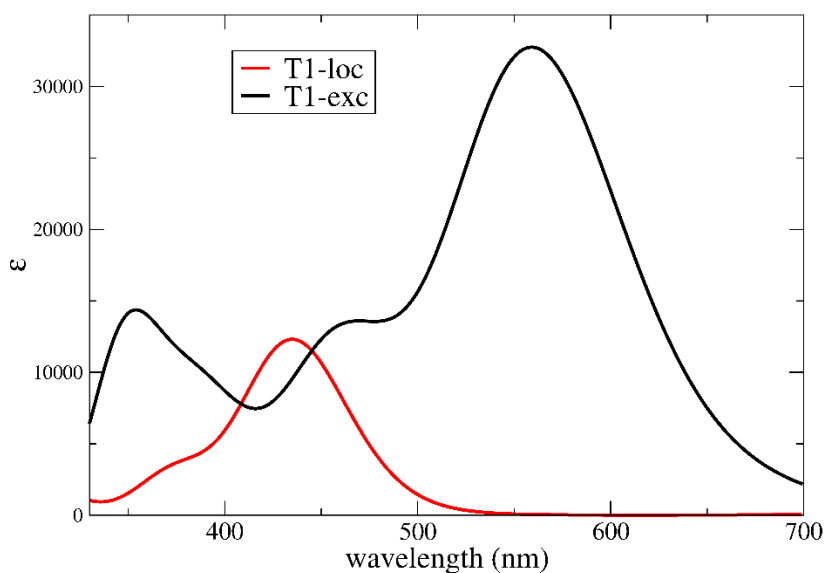


Figure S25. TDA Absorption spectra computed for the 1515_{perp} triplet minima located, T₁-loc-min (red) and T₁-exc-min (black) in DCM. PCM/M052X/6-31+G(d,p) calculations. Spectra simulated by broadening each stick transition with a gaussian with hwhm=0.2 eV

The broadband transient absorption spectra of 1515_{cross} are reported in Figure 5 in the main text. Also in the case, a DADS decaying on the μs time scale is present, whose shape is quite similar to that of the other dinaphthalene species described until now. The most intense band peaks at ~ 450 nm, with a long red-tail until 600 nm.

The simulated absorption spectrum of $T_1\text{-loc-min}$ (see Figure S17 and S18) is similar to the long living component of the experimental one, with a peak just below 400 nm. The spectrum of $T_1\text{-exc-min}$, with three bands at 350, 545 and 600 nm is not instead consistent with the experimental picture. Confirming the indications discussed in the main text, **$T_1\text{-loc-min}$ is thus predicted to be the most stable triplet minimum also for 1515_{cross} .**

4.4. Naphthalene stacked dimer in toluene

The spectra computed at the PCM/ ω B97XD/6-31+G(d,p) level provide a similar picture to that reported in the main text, based on the B2PLYPD3 calculations.

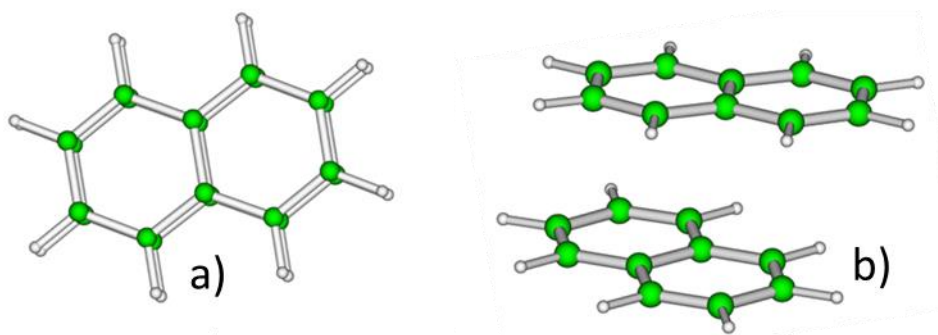


Figure S26. Schematic drawing of a stacked naphthalene dimer in a f2f (a) and in slipped parallel (b) arrangement.

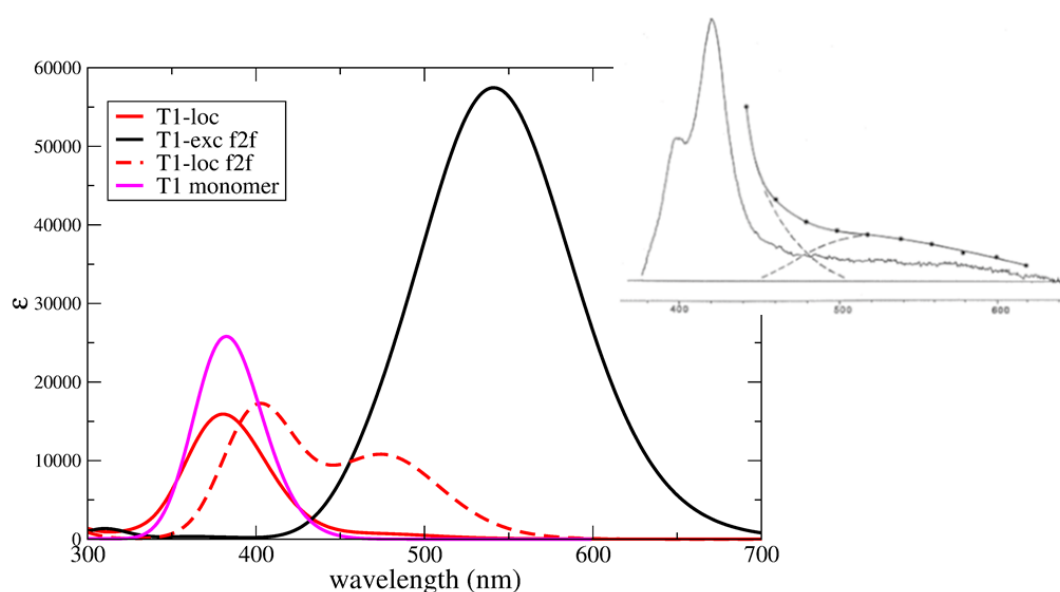


Figure S27. TDA Absorption in toluene. ω B97XD/6-31+G(d,p) with 0.2 broadening. The experimental absorption spectrum of naphthalene in toluene¹⁷ is shown in the inset on the right.

Reference

1. H. Higuchi, K. Tani, T. Otsubo, Y. Sakata and S. Misumi, New Synthetic Method of [2.2]Cyclophanes via Diselena[3.3]cyclophanes, *Bulletin of the Chemical Society of Japan*, 1987, **60**, 4027-4036.
2. R. S. Givens, R. J. Olsen and P. L. Wylie, Mechanistic studies in photochemistry. 21. Photoextrusion of sulfur dioxide: general route to [2.2]cyclophanes, *The Journal of Organic Chemistry*, 1979, **44**, 1608-1613.
3. J. J. Snellenburg, S. Laptinok, R. Seger, K. M. Mullen and I. H. M. van Stokkum, Glotaran: A Java-Based Graphical User Interface for the R Package TIMP, *J. Stat. Softw.*, 2012, **49**, 1 - 22.
4. M. Yamaji, K. Shima, J. Nishimura and H. Shizuka, Laser flash photolysis studies on dynamic behaviour of triplet naphthalenophanes sensitized by triplet benzophenone, *Journal of the Chemical Society, Faraday Transactions*, 1997, **93**, 1065-1070.
5. Y. Zhao, N. E. Schultz and D. G. Truhlar, Design of Density Functionals by Combining the Method of Constraint Satisfaction with Parametrization for Thermochemistry, Thermochemical Kinetics, and Noncovalent Interactions, *J. Chem. Theory Comput.*, 2006, **2**, 364-382.
6. J.-D. Chai and M. Head-Gordon, Long-range corrected hybrid density functionals with damped atom-atom dispersion corrections, *Phys. Chem. Chem. Phys.*, 2008, **10**, 6615-6620.
7. L. Goerigk and S. Grimme, Efficient and Accurate Double-Hybrid-Meta-GGA Density Functionals—Evaluation with the Extended GMTKN30 Database for General Main Group Thermochemistry, Kinetics, and Noncovalent Interactions, *J. Chem. Theory Comput.*, 2011, **7**, 291-309.
8. S. Grimme, S. Ehrlich and L. Goerigk, Effect of the damping function in dispersion corrected density functional theory, *J. Comput. Chem.*, 2011, **32**, 1456-1465.
9. M. E. Sandoval-Salinas, E. Brémond, A. J. Pérez-Jiménez, C. Adamo and J. C. Sancho-García, Excitation energies of polycyclic aromatic hydrocarbons by double-hybrid functionals: Assessing the PBE0-DH and PBE-QIDH models and their range-separated versions, *J. Chem. Phys.*, 2023, **158**, 044105.

10. M. Rodríguez-Mayorga, P. Besalú-Sala, Á. J. Pérez-Jiménez and J. C. Sancho-García, Application to nonlinear optical properties of the RSX-QIDH double-hybrid range-separated functional, *J. Comput. Chem.*, 2024, **45**, 995-1001.
11. J. C. Sancho-García, E. Brémond, A. J. Pérez-Jiménez, I. Ciofini and C. Adamo, Non-empirical double-hybrid density functionals as reliable tools for electronic structure calculations, *Electron. Struct.*, 2022, **4**, 043001.
12. J. Tomasi, B. Mennucci and R. Cammi, Quantum Mechanical Continuum Solvation Models, *Chem. Rev.*, 2005, **105**, 2999-3094.
13. S. Miertuš, E. Scrocco and J. Tomasi, Electrostatic interaction of a solute with a continuum. A direct utilizaion of AB initio molecular potentials for the prevision of solvent effects, *Chem. Phys.*, 1981, **55**, 117-129.
14. J. Cerezo and F. Santoro, FCclasses3: Vibrationally-resolved spectra simulated at the edge of the harmonic approximation, *J. Comput. Chem.*, 2023, **44**, 626-643.
15. M. J. Frisch, G. W. Trucks, H. B. Schlegel, G. E. Scuseria, M. A. Robb, J. R. Cheeseman, G. Scalmani, V. Barone, G. A. Petersson, H. Nakatsuji, X. Li, M. Caricato, A. V. Marenich, J. Bloino, B. G. Janesko, R. Gomperts, B. Mennucci, H. P. Hratchian, J. V. Ortiz, A. F. Izmaylov, J. L. Sonnenberg, Williams, F. Ding, F. Lipparini, F. Egidi, J. Goings, B. Peng, A. Petrone, T. Henderson, D. Ranasinghe, V. G. Zakrzewski, J. Gao, N. Rega, G. Zheng, W. Liang, M. Hada, M. Ehara, K. Toyota, R. Fukuda, J. Hasegawa, M. Ishida, T. Nakajima, Y. Honda, O. Kitao, H. Nakai, T. Vreven, K. Throssell, J. A. Montgomery Jr., J. E. Peralta, F. Ogliaro, M. J. Bearpark, J. J. Heyd, E. N. Brothers, K. N. Kudin, V. N. Staroverov, T. A. Keith, R. Kobayashi, J. Normand, K. Raghavachari, A. P. Rendell, J. C. Burant, S. S. Iyengar, J. Tomasi, M. Cossi, J. M. Millam, M. Klene, C. Adamo, R. Cammi, J. W. Ochterski, R. L. Martin, K. Morokuma, O. Farkas, J. B. Foresman and D. J. Fox, *Gaussian 16 Rev. C.01.Journal*, 2016.
16. F. Neese, Software update: The ORCA program system—Version 5.0, *Wiley Comput. Mol. Sci.*, 2022, **12**, e1606.
17. X. Wang, W. G. Kofron, S. Kong, C. S. Rajesh, D. A. Modarelli and E. C. Lim, Transient Absorption Probe of Intermolecular Triplet Excimer of Naphthalene in Fluid Solutions: Identification of the Species Based on Comparison to the Intramolecular Triplet Excimers of Covalently-Linked Dimers, *J. Phys. Chem. A*, 2000, **104**, 1461-1465.